ISSN 1028-334X, Doklady Earth Sciences, 2006, Vol. 407A, No. 3, pp. 441–445. © Pleiades Publishing, Inc., 2006.
Original Russian Text © M.I. Protasov, V.A. Cheverda, 2006, published in Doklady Akademii Nauk, 2006, Vol. 407, No. 4, pp. 528–532.

GEOPHYSICS

True-Amplitude Seismic Imaging

M. I. Protasov and V. A. Cheverda

Presented by Academician A.S. Alekseev February 10, 2005

Received November 11, 2005

DOI: 10.1134/S1028334X06030214

The objective of our paper is to compute images of reflecting–scattering elements in the investigated geological medium for a given velocity model, i.e., for a model that describes the traveltime of waves with a sufficient degree of accuracy. At present, many approaches exist for computing wave images. Following [1], all of them can be divided into two main (kinematic and dynamic) families. In our work, we shall deal with the dynamic approach. We shall be interested in the procedures for computing the images in true amplitudes, i.e., in amplitudes whose realizations are used to compute images free of the influence of the overlying strata and the system of perturbation and recording (illumination conditions).

The most popular approaches for computing such images were initiated in [2, 3]. They are based on the application of various types of asymptotic decomposition of the Green's function in a nonuniform medium. Up to the present, the most widely used approach is the application of the zero term in ray decomposition. Unfortunately, it is correct only when the ray field is regular. A migration procedure free of this drawback was suggested in [4]. It is based on a representation of the Green's function in the form of a superposition of Gaussian beams. However, this approach is associated with extremely cumbersome calculations. Unfortunately, we are not familiar with its realizations that provide true-amplitude seismic imaging.

In our work, we suggest a procedure for true-amplitude imaging that differs significantly from others, primarily because it is not based on any asymptotic decomposition of the Green's function and it assumes the application of individual Gaussian beams rather than their superposition.

Institute of Geophysics, Siberian Division,
Russian Academy of Sciences, pr. Akademika Koptyuga 3,
Novosibirsk, 630090 Russia; e-mail: chev@uiggm.nsc.ru

FORMULATION OF THE PROBLEM

We assume that the velocity of wave propagation can be presented as a superposition of a smooth component $c_0(x, z)$, which is responsible for the traveltime of the wave and does not cause any variation in its direction, and a sharply varying component $c_1(x, z)$, which does not have any strong influence on the traveltime, but significantly changes its direction (in particular, it determines the return of energy to the free surface). We shall use the Born approximation to describe the reflection–scattering processes occurring at this component of the velocity (see, for example, [3]). The full wave field is presented as a sum of two components,

$$u(x, z; x_s, z_s; \omega) = u_0(x, z; x_s, z_s; \omega) + u_1(x, z; x_s, z_s; \omega),$$

where u_0 is the wave field propagating in a medium described by a smooth component and u_1 is generated by the presence of reflecting–scattering objects, whose images we want to obtain. In the Born approximation, this component of the wave field satisfies the following boundary problem:

$$\Delta u_1 + \frac{\omega^2}{c_0^2(x, z)} u_1 = 2\frac{\omega^2}{c_0^2(x, z)}\frac{c_1(x, z)}{c_0(x, z)} u_0(x, z; x_s, z_s\, \omega);$$

$\left.\dfrac{\partial u_1}{\partial z}\right|_{z = 0} = 0$ are radiation conditions at infinity.

We assume that from hereon the problem of true-amplitude seismic imaging is restoration of the contrast pattern of perturbation of the smooth component of the medium $\dfrac{c_1(x, z)}{c_0(x, z)}$ on the basis of multi-shot multi-offset data:

$$\varphi(x, x_s, \omega) = u_1(x, 0; x_s, 0; \omega).$$

DESCRIPTION OF THE METHOD AND FORMULATION OF THE MAIN RESULT

In order to compute an image at point $(\bar{x}, \bar{z})$ located in a target area, let us initiate a couple of rays from this point in the direction of the free surface using the given

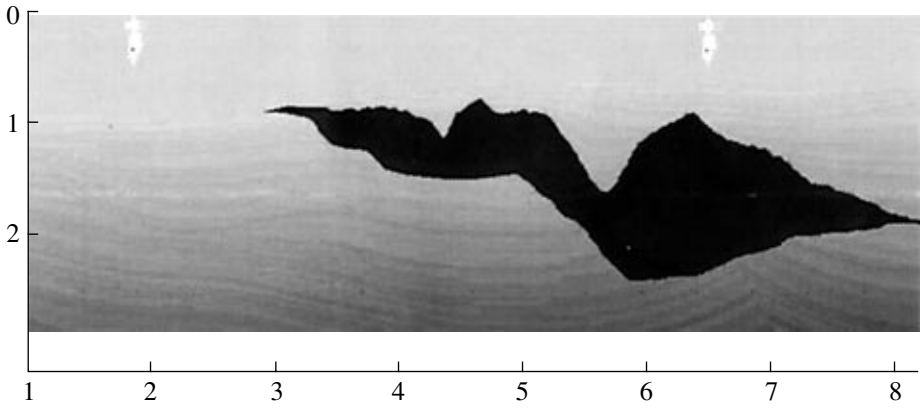

Fig. 1. General view of the SIGSBEE2A model. Here and in Figs. 2 and 4, the distance in axes is given in ft $\times 10^4$.

smooth component $c_0(x, z)$ (Fig. 1). Let us compute a Gaussian beam for each of these rays (see Chapter 8 in [5]) $u^{(gb)}(x, z; \bar{x}, \bar{z}; x_{0g,s}; \omega)$, where $(x_{0g}, 0)$ and (x_{0s}) are points, where the aforementioned rays cross the free surface. We shall discuss the choice of the Gaussian beams later, but we now recall that the Gaussian beam is a specific asymptotic solution of the Helmholtz equation characterized by concentration in the vicinity of a fixed ray and global regularity. Double application of the Green's theorem allows us to obtain the following integral identity:

$$\int_{z=0} \left.\frac{\partial u^{(gb)}(x_s, z; \bar{x}, \bar{z}; x_{0s}; \omega)}{\partial z}\right|_{z=0} dx_s$$

$$\times \int_{z=0} \left.\frac{\partial u^{(gb)}(x_s, z; \bar{x}, \bar{z}; x_{0g}; \omega)}{\partial z}\right|_{z=0} \varphi(x, x_s, \omega) dx$$

$$= 2\omega^2 F(\omega) \iint_{z>0} \frac{1}{c_0^2(\xi, \eta)} \frac{c_1(\xi, \eta)}{c_0(\xi, \eta)}$$

$$\times u^{(gb)}(\xi, \eta; \bar{x}, \bar{z}, x_{0s}; \omega) u^{(gb)}(\xi, \eta; \bar{x}, \bar{z}, x_{0g}; \omega)\, d\xi\, d\eta. \quad (1)$$

Let us now describe the choice of the Gaussian beams used in Eq. (1). It is known (Chapter 8 in [5]) that a Gaussian beam in the ray system of coordinates (s, q) is specified in the following form:

$$u^{(gb)}(s, q; \omega) = \sqrt{\frac{c_0(s, 0) Q(s_0)}{c_0(s_0, 0) Q(s)}}$$

$$\times \exp\{i\omega\tau(s)\} \exp\left\{\frac{i\omega}{2}\Gamma(s) q^2\right\}.$$

Below, we shall consider that the ray length is calculated from the free surface into the interior of the medium. It is equal to s_0 at the internal point $(\bar{x}, \bar{z})$. Now, $\Gamma(s) = P(s)Q^{-1}(s)$, where functions $Q(s)$ and $P(s)$ satisfy the following system of ordinary differential equations:

$$\frac{dQ}{ds} = c(s, 0) P, \quad \frac{dP}{ds} = -\frac{1}{c_0^2(s, 0)} \left.\frac{\partial^2 c_0}{\partial q^2}\right|_{q=0} Q,$$

$$Q(s_0) = Q_0, \quad P(s_0) = P_0$$

and the additional condition

$$\bar{Q}(s_0) P(s_0) - \bar{P}(s_0) Q(s_0) = i\frac{k}{\omega}$$

with dimensionless constant k, which governs the width of the Gaussian beam. In all further considerations, initial data Q_0 and P_0 are selected to provide the minimal beam width precisely at that point where imaging is performed.

Now we shall use the concentration of the Gaussian beams in a near neighborhood of the ray to reduce the integration in the right part of Eq. (1) to integration over a small neighborhood of point $(\bar{x}, \bar{z})$. Neglecting the variability of the smooth component of the velocity structure in this neighborhood, we can use explicit relations for representing the Gaussian beams in a polar coordinate system with the center at the selected point:

$$u^{(gb)}_{0g(s)}(\xi, \eta; \bar{x}, \bar{z}; x_{0g(s)}; \omega)$$

$$= \exp\left\{i\omega\left[\tau_{0g(s)}(\bar{x}, \bar{z}) - \frac{\rho\cos(\varphi - \varphi_{0g(s)})}{c_0(\bar{x}, \bar{z})}\right]\right\}$$

$$\times \exp\left\{-\frac{i\omega}{2c_0(\bar{x}, \bar{z})} \frac{\rho^2 \sin^2(\varphi - \varphi_{0g(s)})}{\rho\cos(\varphi - \varphi_{0g(s)}) + \frac{ik}{2}\frac{c_0(\bar{x}, \bar{z})}{\omega}}\right\},$$

where $\tau_{0g(s)}(\bar{x}, \bar{z})$ denotes traveltime of the wave from the current point $(\bar{x}, \bar{z})$ to point $(x_{0g(s)}, 0)$ at the free sur-

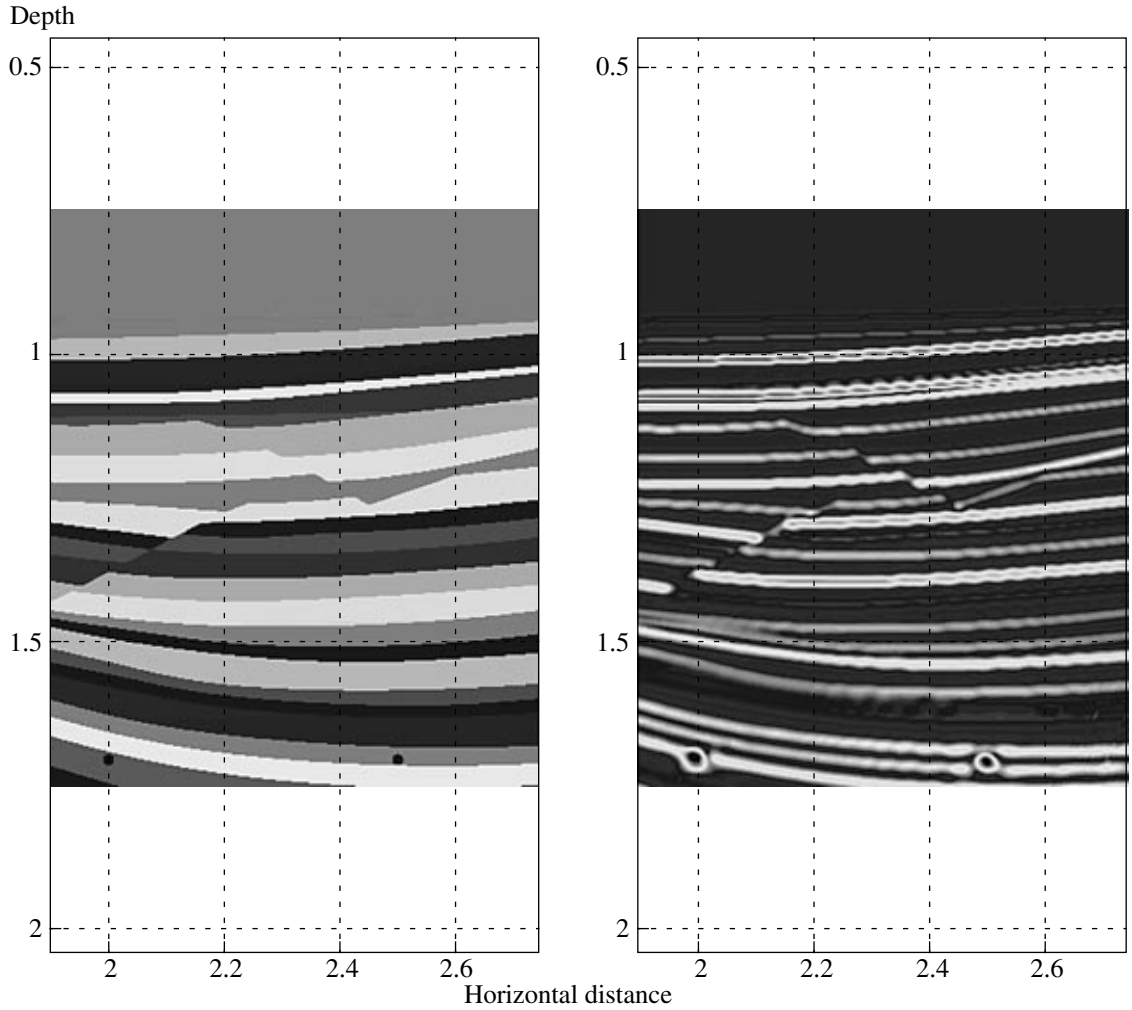

Fig. 2. Restored (on the right) and true (on the left) structures of the location of reflecting levels in the SIGSBEE2A model for the salt inclusion-free region.

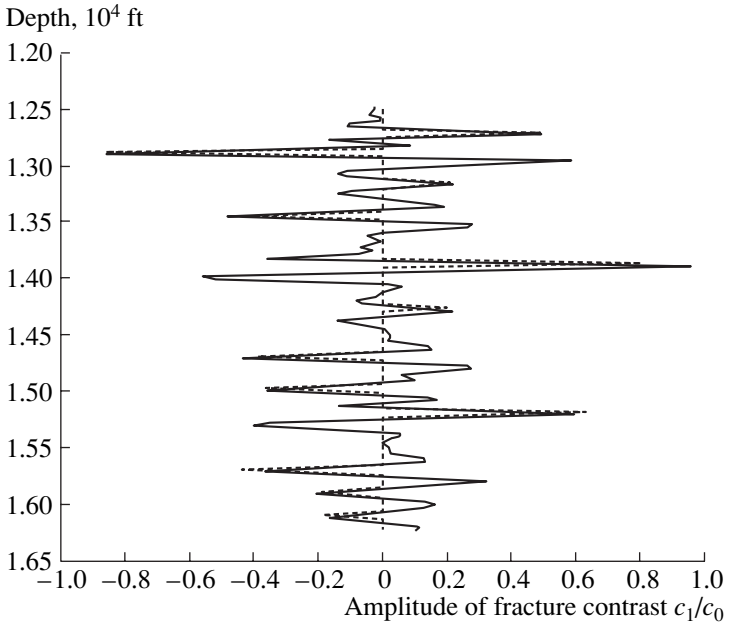

Fig. 3. Restored (solid line) and true (dashed line) reflectivity of the model along a vertical section at $x = 22000$ *ft.*

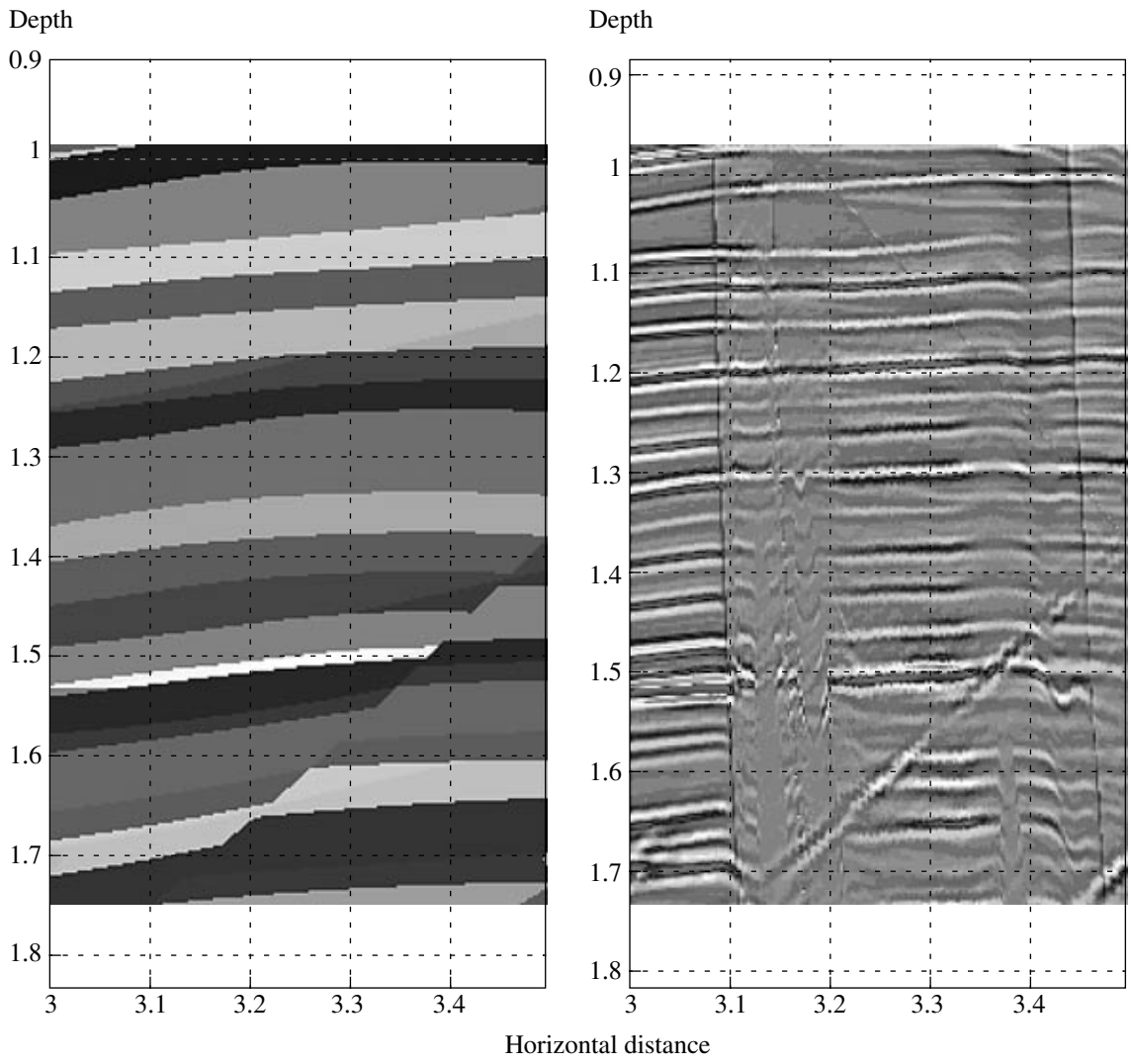

Fig. 4. Restored (on the right) and true (on the left) velocity structure beneath the left flank of the salt inclusion.

face. Now, it is not difficult to obtain the main integral identity that determines the true-amplitude imaging:

$$\Phi(\bar{x}, \bar{z}; \varphi_{0g}, \varphi_{0s}) \overset{\text{def}}{=}$$

$$= \left| \int_\omega \exp\{-i\omega(\tau_{0g}(\bar{x}, \bar{z}) + \tau_{0s}(\bar{x}, \bar{z}))\} d\omega \right.$$

$$\times \int_{z=0} \left. \frac{\partial u_{0s}^{(gb)}(x_s, z; \bar{x}, \bar{z}; x_{0s}; \omega)}{\partial z} \right|_{z=0} dx_s,$$

$$\int \left. \frac{\partial u_{0g}^{(gb)}(x_s, z; \bar{x}, \bar{z}; x_{0g}; \omega)}{\partial z} \right|_{z=0} \varphi(x, x_s, \omega) dx_s \Big|$$

$$= \left| \frac{2}{c_0^2(\bar{x}, \bar{z})} \int_0^R d\rho \int_0^{2\pi} K(\rho, \varphi; \varphi_{0g}, \varphi_{0s}) \right.$$

$$\left. \times \frac{c_1(\bar{x} + \rho\cos\varphi, \bar{z} + \rho\sin\varphi)}{c_0(\bar{x} + \rho\cos\varphi, \bar{z} + \rho\sin\varphi)} d\varphi \right|. \quad (2)$$

This is indeed a true-amplitude imaging, because the right-hand part of Eq. (2) includes an averaging of the perturbation contrast of the surrounding medium with the following kernel:

$$K(\rho, \varphi; \varphi_{0g}, \varphi_{0s}) = \int_\omega F(\omega)$$

$$\times \exp\left\{ -i\omega\rho \frac{\cos(\varphi - \varphi_{0g}) + \cos(\varphi - \varphi_{0s})}{c_0(\bar{x}, \bar{z})} \right\}$$

$$\times \exp\left\{ -\frac{i\omega\rho^2}{2c_0(\bar{x}, \bar{z})} \left(\frac{\sin^2(\varphi - \varphi_{0g})}{\rho\cos(\varphi - \varphi_{0g}) + \frac{ik}{2}\frac{c_0(\bar{x}, \bar{z})}{\omega}} \right. \right.$$

$$+\frac{\sin^2(\varphi-\varphi_{0s})}{\rho\cos(\varphi-\varphi_{0s})+\frac{ik}{2}\frac{c_0(\bar{x},\bar{z})}{\omega}}\Bigg)\Bigg\}d\omega, \qquad (3)$$

which does not depend on the structure of the overlying column and is fully determined by the spectrum of the sounding signal, selected geometry of the rays, and local properties of the surrounding medium.

DESCRIPTION OF NUMERICAL EXPERIMENTS

Synthetic data for the SIGSBEE2A model placed at our disposal by the SMAART Company were used for the numerical experiments.[1] The general shape of the model is shown in Fig. 1. The objective of processing is to determine the detailed structure of this model (thin layers, fractures, pinchouts, and location of point scatterers) especially under a salt inclusion. It is worth noting that, currently, these synthetic data are a specific touchstone designed for testing new approaches to the solution of an inverse problem of the theory of wave propagation for especially complex models of media. Our main objective in their processing was to demonstrate the efficiency of the suggested approach for realistic models of different media.

Figure 2 presents restored (on the right) and true (on the left) parts of the SIGSBEE2A model related to the salt intrusion-free region. One can clearly see the coincidence between true and restored boundaries of the interface, location of fractures, and solitary scattering objects specially included into the model. In order to estimate the accuracy of the restored contrasts of the perturbation in the surrounding medium, we present Fig. 3, in which the restored and true reflectivity patterns of the medium along vertical line $x = 22000$ ft are shown. From hereon, we understand reflectivity as the normalized value of velocity discontinuity.

[1] These data are freely available at <smaart2-admin@chevron.com>.

It is noteworthy that along with insignificant displacement of the boundaries caused by the application of a smoothed model instead of a stratigraphic one, there are also false increases in the amplitudes unrelated to any reflecting–scattering objects. In our opinion, their appearance is caused by the fact that the averaging kernel has an oscillating character. Hence, imaging of any fraction would be accompanied by fluctuations of amplitudes at its boundaries, and the amplitude of these oscillations would positively correlate with the fracture amplitude. However, as one can see from Fig. 3, the amplitudes of the main oscillations coincide quite well with the amplitude of the fractures.

The result of application of this approach to imaging the subsalt structure is shown in Fig. 4. One can clearly see two bands of image aberration related to the diffraction of the Gaussian beams at the left flank of the salt body. At the same time, this approach is undoubtedly successful; one can see a clear image of the fracture in the subsalt region and an absolutely correct image of the thin layered structure immediately beneath the left flank of the salt body at a depth interval of 10 000–14 000 ft.

ACKNOWLEDGMENTS

The authors thank the SMAART Joint Association for providing the synthetic data set for the SIGSBEE2A model. This study was supported by the Moscow Scientific Center of the Schlumberger Company and the Russian Foundation for Basic Research, (project nos. 04-05-64177 and 05-05-64277).

REFERENCES

1. P. Hubral, J. Schleicher, and M. Tygel, Geophysics **61**, 742 (1996).
2. N. Bleistein, Geophysics **52**, 931 (1987).
3. G. Beylkin, J. Math. Phys. **26**, 99 (1985).
4. N. R. Hill, Geophysics **66**, 1240 (2001).
5. V. M. Babich and V. S. Buldyrev, *Asymptotic Methods in the Problems of Shortwave Diffraction* (Nauka, Moscow, 1972) [in Russian].